Surface-induced self-assembly of amphiphilic block copolymers into functional bilayer thin films

Jean-Paul Chapel, Christophe Schatz, Fabrice Cousin, Thierry Buffeteau, Martin Fauquignon, Alliny F Naves, Flavia Mesquita Cabrini

Surface-induced Self-Assembly of Amphiphilic Block Copolymers into Functional Bilayer Thin Films.

Flávia M. Cabrini[1,2], Alliny F. Naves[1], Martin Fauquignon[2], Thierry Buffeteau[3], Fabrice Cousin[4], Christophe Schatz[2], Jean-Paul Chapel[1]

[1]*Centre de Recherche Paul Pascal (CRPP), UMR CNRS 5031, Université de Bordeaux*

[2]Laboratoire de Chimie des Polymères Organiques (LCPO), Université de Bordeaux, Bordeaux INP, UMR CNRS 5629
[3]Laboratoire Léon Brillouin, Université Paris-Saclay, UMR 12, CEA-CNRS, 91191 Gif Sur Yvette, France
[4]Université de Bordeaux, CNRS, Bordeaux INP, ISM, UMR 5255, 33400 Talence, France

Self-assembly, amphiphilic block copolymers, bilayer, thin organic film, solvent shifting, surface

ABSTRACT: An scalable method for the fabrication of symmetric and asymmetric BC bilayers on solid support of any type, shape and size is proposed, in order to overcome the specific limitations of currently available techniques (notably Langmuir-Blodgett (LB) deposition and polymersome vesicle fusion (VF)). We demonstrated that this fabrication process is viable by developing a proof of concept on silicon wafers, flat and macroscopic substrates that allow the use of a wide range of complementary state-of-the-art techniques to precisely characterize the different steps of the assembly. This type of assembly, however, is potentially possible on colloidal objects, as showed by preliminary results. The proposed fabrication method was done using polystyrene-*block*-poly(acrylic acid) block copolymer and consists of two steps: i) the formation of a monolayer of BCs by the establishment of non-covalent interactions between the substrate and the hydrophilic blocks in a non-selective solvent ii) the controlled addition of a selective solvent (water) which triggers the assembly of the second layer through hydrophobic interactions between the free and previously adsorbed hydrophobic blocks resulting in the formation of a self-assembled bilayer of BCs on a solid support. A final rinsing step allows to eliminate the excess of aggregates (micelles) generated in the solution during the second step. BC monolayers and bilayers on solid supports were obtained and characterized using various surface characterization techniques. The ability of these bilayers to encapsulate hydrophobic actives of interest for specific applications has also been highlighted using gold nanoparticles (AuNPs). Finally, the possibility to form asymmetric bilayers was demonstrated on a PS-*b*-PAA/PS-*b* -poly(vinyl pyridine) (PS-b-P2VP) system.

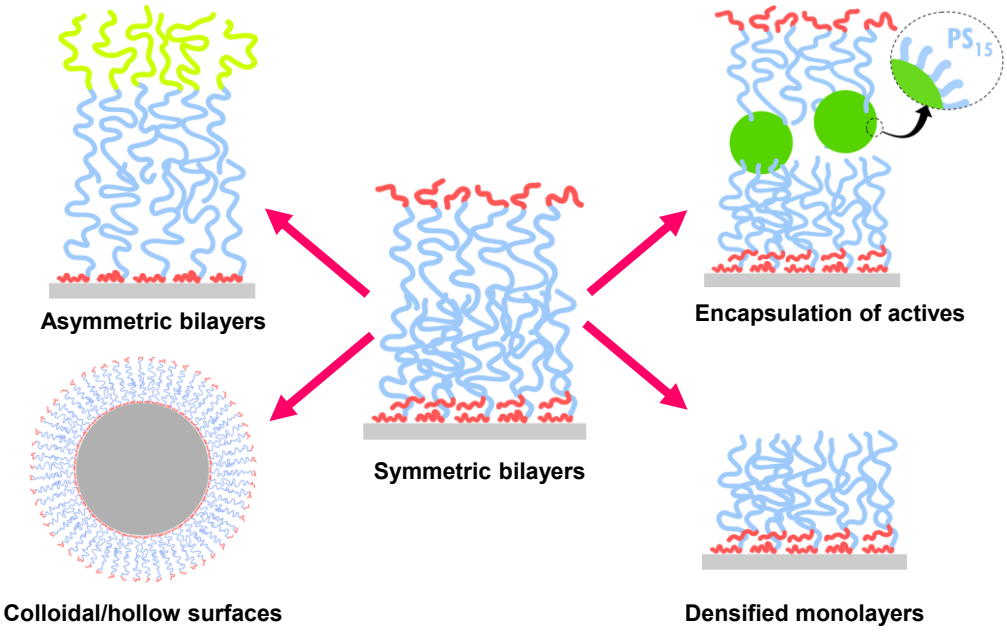

TOC

1. INTRODUCTION

Block copolymers (BCs) are widely used in materials science due to their capacity to self-assemble, in bulk, thin film or solution into a variety of nanoscale ordered structures with different morphologies.[1-13] In particular the ease of amphiphilic BCs to form bilayer membranes in solution has attracted much interest over the past 20 years as shown by the vast literature on polymer vesicles (polymersomes).[14,15] More recently, solid-supported BC bilayers have also been put forward.[16-18] Although they share similar morphologies with the popular lipid-supported membranes used as models of biomimetic interfaces, it is well-established through studies on liposomes and polymersomes that BCs form much more stable membranes than conventional lipids owing to a partial interpenetration of the individual membrane layers minimizing any delamination.[19,20] Furthermore, the larger hydrophobic reservoir offered by BC bilayers is a key advantage for the encapsulation of actives (molecules, or nanoparticles) over the typically smaller reservoirs of lipid membranes.

Applications of solid-supported BC bilayers are currently poorly investigated owing to the difficulty to generate them in good conditions at a large scale and/or on non-planar substrates with current methods Notably, the Langmuir-Blodgett (LB) and the Langmuir-Schaefer (LS) deposition techniques are powerful lab scale methods to build BC bilayers at high resolution with negligible defects.21,22 Unfortunately, the LB/LS approaches cannot be satisfactorily implemented at large scale or on colloidal and hollow structures. Besides, the vesicle fusion (VF) which is the standard method for liposomes to produce continuous lipid bilayers suffers from certain limitations when applied to polymersomes. Notably, the mechanical robustness of polymer vesicles prevents their rupture and fusion in the absence of strong attractive interaction with the surface.23-25 The more recently solvent-assisted lipid bilayer (SALB) pathway is an alternative to the VF method where a lipid solution prepared in a water-miscible organic solvent is deposited on a solid substrate, followed by gradual exchange with water to generate lamellar-phase structures, leading to the formation of supported lipid bilayers.26-29 However, in the absence of specific interaction with the substrate, this method can hardly apply to BCs to form homogeneous bilayers anchored to the surface. Additionally, VF and SALB methods are restricted to block copolymers having geometry properties that fit with the formation of vesicles ($\frac{1}{2} < \rho < 1$) or lamellar structures ($\rho \sim 1$) with ρ the packing parameter.10,30

Moving towards a universal fabrication of solid-supported BC bilayers, we report a simple and robust bottom-up approach able to generate symmetrical and asymmetrical bilayers on solid substrates of any size and shape without strict restriction on the ρ value. For this purpose, amphiphilic diblock copolymers with one adsorbing hydrophilic block and one non-adsorbing hydrophobic block are used. The proposed two-step method, reminiscent of the layer-by-layer approach used with polyelectrolytes[31] is based on i) the formation of a first BC layer through the build-up of non-covalent interactions between the substrate and the hydrophilic blocks in a non-selective solvent like THF or DMF and ii) the triggered assembly of the second layer through hydrophobic interactions between free and grafted hydrophobic blocks by adding a critical water fraction in the medium (**Figure 1**). A final rinsing step allows then to remove the excess BC micelles, vesicles and any aggregates generated in the aqueous solutions during the second step. Basically, the overall pathway reproduces at the solid-liquid interface the hydrophobically-driven self-assembly mechanism of amphiphilic BCs in solution.

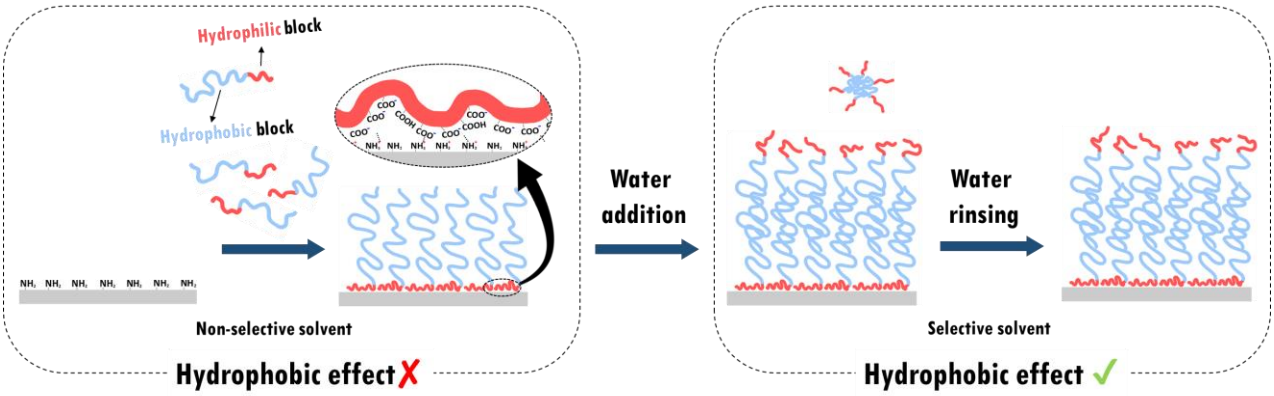

Figure 1. General scheme of the surface self-assembly of amphiphilic BCs into solid-supported bilayers.

While the proof of concept was previously reported with BC forming bilayer around polyelectrolyte complex particles,[32] we aim here to standardize the self-assembly process by performing a thorough study on model planar substrates. BCs containing vitreous and hydrophobic polystyrene blocks have been selected as model system due to their reputation to be difficult to assemble through conventional approaches like vesicle spreading. We also report, the successful formation of asymmetric bilayers, particle coating with BC bilayers and the immobilization of gold nanoparticles either in the hydrophobic reservoir or at the surface of the top layer, as a first evidence of the capacity of the BC bilayers to sequestrate colloidal objects. Solid-supported lipid bilayers have been mainly used to study *in vitro* membrane-related processes. BC bilayers can offer additional features as robust organic thin films with on-demand surface functionality, an appealing capacity of encapsulating actives and a compatibility with different physicochemical environments. In this regard, the 'surface-induced' self-assembly of BCs as described herein enriches the panel of directed self-assembly approaches used to design functional organized ultrathin films.[11,31,33]

2. EXPERIMENTAL SECTION

Adsorption of a BC monolayer at the wafer surface: The APTES- or PAH-modified wafers were immersed in a rectangular Teflon trough filled with 8 mL of BC solution in DMF:THF (80:20, v/v) prepared at various concentrations and filtered on 0.1 µm PTFE membrane. After 2h, the wafers were rinsed in a DMF:THF mixture to remove excess of BC and gently dried under a nitrogen flow.

Self-assembly of the BC bilayer at the wafer surface: The APTES-modified wafers were first immersed in the trough containing the BC solution in similar conditions as those used for the BC monolayer. Water was then slowly added with a syringe pump (New Era, NE-300) at a rate of 50 µL.min^{-1} until a water content of 7 vol. % was reached. The system was allowed to equilibrate for a defined period of time comprised between 1 and 72 h. Afterward, the simultaneous injection of DI water at one end and the withdrawal of the solution at the other were performed with two syringe pumps at increasing flow rates (300 µL.min^{-1} during 2 h followed by 5 mL.min^{-1} during 5 min) to fully exchange the BC solution with pure water. The wafer substrates with the BC bilayer were then taken out carefully and dried under a nitrogen flow. Specifically, to minimize capillary forces at the air/water interface, the wafers were slowly removed vertically from the solution.

Ellipsometry: Bilayer thicknesses on silicon wafers and sensors were measured by using UVISEL spectroscopic ellipsometer (Horiba Jobin Yvon, France). The data were acquired at three angles of incidence: 65°, 70° and 75° at wavelengths ranging from 260 to 860 nm. Data were fitted to a multi-layer model using the DeltaPsi Horriba built-in program. The thicknesses obtained through spectroscopic ellipsometry was systematically confirmed by AFM measurements. Several scratches were made on the polymer layer deposited on both silicon wafers and QCM sensors by pulling (and not cutting) sideway a sharp surgical scalpel blade and then imaging the generated scratches to estimate the film thickness (step height) as shown in Figure SX.

Quartz Crystal Microbalance with dissipation A QCM-D set-up (Q-Sense E4 instrument, Biolin Scientific, Sweden) with home-made amino-modified quartz crystal sensors (either with APTES or PAH) was used to monitor the adsorption isotherm of the PS-*b*-PAA copolymers in good solvent conditions. The adsorption of polymer chains on a sensor can be precisely monitored by measuring the decrease in the resonance frequency F_n for each odd overtone. If the adsorbed mass is forming a rigid homogeneous lossless film, the relation between frequency change ΔF_n and the areal mass increment Δm is linear, as found by Sauerbrey[4] (Eq. 1):

$$\frac{\Delta F_n}{n} = -\frac{2F_0^2}{\sqrt{\rho_q \mu_q}} . \Delta m \qquad \text{Eq.1}$$

where F_o is the resonant frequency of the crystal (5 MHz), ρ_q (2.648 g.cm^{-3}) the quartz density and μ_q (2.947 x 10^{11} g.cm^{-1} s^{-2}) the shear modulus. The original silicon tubing of the QCM setup was replaced by Teflon-based because they offered a better resistance in THF and DMF solvents (no swelling). The solutions were injected using a push/pull style syringe pump. A flow rate of 150 µL.min^{-1} was used for each BC injection and solvent rinsing. After the injection of the BC at a given concentration, the real time monitoring was conducted until no significant differences in frequency were observed. As a result, the waiting time between consecutive injections of BCs solutions with different concentrations is not fixed and depends on the time required to reach this plateau.

Advancing water contact angles: Advancing and receding water contact angles (θ_{adv}, θ_{rec}) were measured with a Tracker tensiometer from Teclis (France) at room temperature. The static contact angle was recorded using the sessile drop method at room temperature. With the help of a dosing syringe, a droplet of 3 µL of water (pH 7) was deposited on the substrate and the value of advancing contact angle was recorded at 30 s after the droplet was set. The average value was obtained by measuring the two samples in two different positions each. The natural receding contact angles were determined by monitoring the evaporation of the sessile drop with time: a contact angle initially imposed in the advancing mode (θ_A) diminishes and tends towards a receding value (θ_R) when the liquid constituting the meniscus start to evaporate.[5,6]

AFM: AFM images of bilayers were recorded either in the dry state by using Tapping Mode in Air at a resolution of 512 x 512 pixels with a scan rate of 1 Hz with a Dimension ICON (Veeco, Bruker) and in the wet state (water) using Peak Force Mode at similar resolution and scan rates with a Bioscope Resolve (Bruker). For the wet state analysis, a droplet of the liquid

was placed at the AFM tip and surface of the bilayer to then engage and image. Unless stated otherwise, the AFM images shown were obtained using Tapping Mode in Air. All the data was analysed with Nanoscope Analysis software.

Neutron Reflectivity: The Neutron reflectivity measurements were performed on the time-of-flight reflectometer

HERMES at the Laboratoire Léon Brillouin (LLB). Two geometries were used. In the first one the silicon/air interface was probed with a q-range varying from 0.008 to 0.07 $Å^{-1}$. In the second one, the silicon/deuterated toluene interface was probed (the neutron getting through the sample) with a q-range varying from 0.01 to 0.08 $Å^{-1}$. A specific home-made cell was used to perform the experiments in d-THF. During the experiment, we use all the wavelengths provided by the neutron source from 3 Å to 25 Å with a constant Dl of 0.3 Å. We use for the silicon/air interface q = 0.93° and for the silicon/deuterated THF q = 1.23° with a Dq of 0.05°. The experimental resolution is taken into account in the fitting procedure (Motorfit).

PM-IRRAS: The PM-IRRAS spectra were recorded on a ThermoNicolet Nexus 670 FTIR spectrometer at a resolution of 4 cm^{-1}, by co-adding several blocks of 1500 scans (30 min acquisition time). Generally, eight blocks (4 h acquisition time) were necessary to obtain PM-IRRAS spectra of ultrathin films or SAMs with good signal-to-noise ratios. Experiments were performed at an incidence angle of 75° using an external homemade goniometer reflection attachment.[7] As shown in Figure 1, the infrared parallel beam (modulated in intensity at frequency f_i lower than 5 KHz) was directed out of the spectrometer with an optional flipper mirror and made slightly convergent with a first BaF_2 lens (191 mm focal length). The IR beam passed through a BaF_2 wire grid polarizer (Specac) to select the p-polarized radiation and a ZnSe photoelastic modulator (PEM, Hinds Instruments, type III). The PEM modulated the polarization of the beam at a high fixed frequency, $2f_m$=100 KHz, between the parallel and perpendicular linear states. After reflection on the sample, the double modulated (in intensity and in polarization) infrared beam was focused with a second ZnSe lens (38.1 mm focal length) onto a photovoltaic MCT detector (Kolmar Technologies, Model KV104) cooled at 77 K. The polarization modulated signal I_{AC} was separated from the low frequency signal I_{DC} (f_i between 500 and 5000 Hz) with a 40 KHz high pass filter and then demodulated with a lock-in amplifier (Stanford Model SR 830). The output time constant was set to 1 ms. The two interferograms were high-pass and low-pas filtered (Stanford Model SR 650) and simultaneously sampled in the dual channel electronics of the spectrometer. In all experiments, the PEM was adjusted for a maximum efficiency at 2500 cm^{-1} to cover the mid-IR range in only one spectrum. For calibration measurements, a second linear polarizer (oriented parallel or perpendicular to the first preceding the PEM) was inserted between the sample and the second ZnSe lens. This procedure was used to calibrate and convert the PM-IRRAS signal in terms of the IRRAS signal (*i.e.* 1 – $(R_p(d)/R_p(o)$, where $R_p(d)$ and $R_p(o)$ stand for the p-polarized reflectance of the film/substrate and bare substrate systems, respectively).[8,9]

3. RESULTS AND DISCUSSION

3.1 Monolayer formation

The first step towards the self-assembly of solid-supported bilayers relies on the formation of a BC monolayer through specific interactions between the substrate and copolymer molecules in a non-selective solvent. For this purpose, poly(styrene)-b-poly(acrylic acid) copolymers (PS-b-PAA) containing relatively short PAA blocks and large PS blocks, were adsorbed onto silicon wafers modified with amino groups either through covalent grafting of 3-(aminopropyl)-triethoxysilane (APTES) or non-covalent grafting of polyallylamine hydrochloride (PAH) (**ESI, S1**). BC adsorption was achieved in DMF:THF

(80:20, v:v) where PS-b-PAA chains are well solvated and therefore cannot self-assemble (**ESI, S1**). The PAA blocks can however strongly interact with amino groups through acid-base interactions generating ion pairs ($–COO^-/–NH_3^+$) at silica surface. This was evidenced by PM-IRRAS spectroscopy where the presence of a strong band at 1570 cm^{-1} corresponding to the symmetric stretching of -COO^- groups indicated that -COOH groups have deprotonated upon interaction with amine; a deprotonation degree of 60% was derived based on the respective optical indexes of the protonated and non-protonated forms of acrylic acid (**Figure 2**). Since PS blocks cannot adsorb on silica under similar solvent conditions,[34] BC chains must adopt an anchor-and-buoy conformation where the short adsorbing PAA blocks (anchor) fix one end of the rather long non-adsorbing PS blocks (buoy) close to the surface. More specifically and according to the scaling description of BC adsorption from non-selective solvent, the structure of the polymer layer is determined by the block asymmetry ratio, $\beta = (R_{F,B}/R_{F,A}) = (N_B/N_A)^{3/5}$ where R_F is the Flory radii in good solvent conditions, N the degree of polymerization, A and B referring to the anchor and buoy blocks.[35-37] When $\beta > N_A^{1/2}$, the adsorption is moderated by lateral repulsion between the buoys blocks; when $1 < \beta < N_A^{1/2}$, the adsorption is limited by the saturation of the surface by the anchor blocks. According to the BC compositions, all systems considered here are expected to fall into the second case, i.e. the anchor-dominating regime.

With water contact angle values close to 70° the BC monolayer has a relative weak hydrophobic character compared to that expected for polystyrene (θ=88°).[38] It attests of a physical and/or chemical heterogeneity as indicated by the relatively high value of hysteresis ($\Delta\theta > 25°$)[39] (**Table 1**).

AFM analysis of the monolayer in air after removal of excess copolymer revealed a periodic two-dimensional pattern of islet structures resulting from the dewetting of PS blocks on the adsorbed PAA layer during the passage of the substrate at the liquid-air interface, as previously reported for the adsorption of PS-b-P2VP on mica.[40] The average size of as-formed PS clusters increased with increasing PS block size due to greater chemical incompatibility with PAA (Figure 2). Importantly, the nature of the amine groups grafted on the wafer (APTES or PAH) has no influence on the segregation behaviour of PS, nor the solvent used (DMF, THF or a mixture) or the drying method (fast drying with nitrogen or slow drying by solvent evaporation) (**ESI, SX**). The clusters were no longer discernible when the monolayer was immersed in toluene, which is a good solvent of PS, or exposed to saturated atmosphere of toluene (**Figure 2**). QCM-d and neutron reflectivity (NR) were used to provide a quantitative description of BC adsorption in non-selective solvent. Among the most important findings, we can emphasize that the adsorption was characterized by a large adsorption constant (K) that reflects the strength of the multivalent interaction between acid and amino groups at surface. Besides, the grafting density (σ) obtained from the saturation plateau in the isotherms (Γ_{sat}) follows as expected for the anchor-dominating regime (**ESI, S2**).[35,36] Regarding the thickness (δ) of the adsorbed layer in good solvent conditions, NR analysis performed in THF provided δ values of 14.5 and 18.5 nm for PS_{182}-b-PAA_{19} and PS_{394}-b-PAA_{58}, respectively (**ESI, S2**). By neglecting the thickness of the anchoring layer, it implies that on average PS chains are stretched up to 32% and 19% of the extended all-trans conformation (bond length of 1.54 Å and tetrahedral angles of 109.28).[41] The highest stretching is expected for $\beta = N_A^{1/2}$ which is the cross-over between the buoy and anchor regime.[36] The thickness of the monolayer scaled as $\delta \sim N_B\sigma^{1/3}$, in line with the prediction for the anchor-dominated adsorption (**ESI, S2**).[35,36] This is also consistent with the Alexander-de Gennes formalism of a terminally attached brush.[42-45] In this regime, the equilibrium height of the brush is a balance of interaction energy and elastic free energy.[46] The distance between the grafted points ($D = \sigma^{-1/2}$) was found to be smaller than the radius of gyration (R_g) of the PS chains in good solvent,[47] confirming the brush regime for PS (**ESI, S2**).

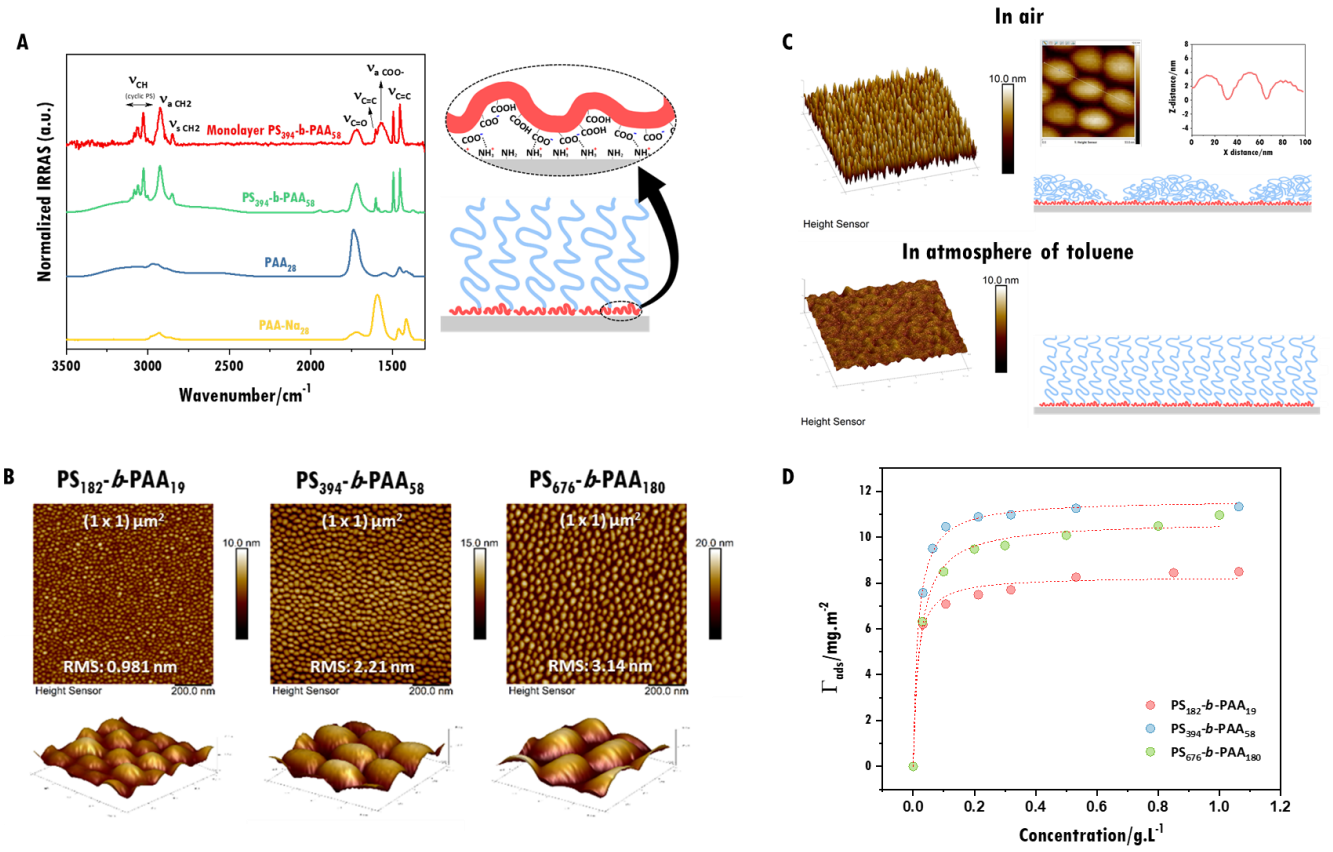

Figure 2. A. Normalized PM-IRRAS spectra of the PS_{394}-b-PAA_{58} monolayer with spin-coated PS_{394}-b-PAA_{58}, PAA_{69} (acid form) and PAA_{69} (salt form). (d) Schematic representation of proposed acid-base interaction between the amino groups at the surface with the carboxylate groups from the hydrophilic PAA block. B. AFM images of PS-b-PAA monolayers in air. C. AFM images of the monolayer of PS_{394}-b-PAA_{58} in dry and atmosphere saturated with non-selective solvent conditions. D. Adsorption isotherm of PS_{394}-b-PAA_{58} onto the substrate pre-functionalized with APTES.

Table 1. Water contact angle values for the dried monolayers.

	θ_A	θ_R	$\Delta\theta$
PS_{182}-*b*-PAA_{19}	67°	43°	25°
PS_{394}-*b*-PAA_{58}	66°	33°	33°
PS_{677}-*b*-PAA_{180}	68°	39°	29°

AFM analysis of the monolayer in air after removal of excess copolymer revealed a periodic two-dimensional pattern of islet structures resulting from the dewetting of PS blocks on the adsorbed PAA layer during the passage of the substrate at the liquid-air interface, as previously reported for the adsorption of PS-b-P2VP on mica.[40] The average size of as-formed PS clusters increased with increasing PS block size due to greater chemical incompatibility with PAA (**Figure 2**). Importantly, the nature of the amine groups grafted on the wafer (APTES or PAH) has no influence on the segregation behaviour of PS, nor the solvent used (DMF, THF or a mixture) or the drying method (fast drying with nitrogen or slow drying by solvent evaporation) (**ESI, SX**). The clusters were no longer discernible when the monolayer was immersed in toluene, which is a good solvent of PS, or exposed to saturated atmosphere of toluene (**Figure 2**). QCM-d and neutron reflectivity (NR) were

used to provide a quantitative description of BC adsorption in non-selective solvent. Among the most important findings, we can emphasize that the adsorption was characterized by a large adsorption constant (K) that reflects the strength of the multivalent interaction between acid and amino groups at surface. Besides, the grafting density (σ) obtained from the saturation plateau in the isotherms (Γ_{sat}) follows as expected for the anchor-dominating regime (**ESI, S2**).[35,36] Regarding the thickness (δ) of the adsorbed layer in good solvent conditions, NR analysis performed in THF provided δ values of 14.5 and 18.5 nm for PS_{182}-b-PAA_{19} and PS_{394}-b-PAA_{58}, respectively (**ESI, S2**). By neglecting the thickness of the anchoring layer, it implies that on average PS chains are stretched up to 32% and 19% of the extended all-trans conformation (bond length of 1.54 Å and tetrahedral angles of 109.28).[41] The highest stretching is expected for $\beta = N_A^{1/2}$ which is the cross-over between the buoy and anchor regime.[36] The thickness of the monolayer scaled as $\delta \sim N_B\sigma^{1/3}$, in line with the prediction for the anchor-dominated adsorption (**ESI, S2**).[35,36] This is also consistent with the Alexander-de Gennes formalism of a terminally attached brush.[42-45] In this regime, the equilibrium height of the brush is a balance of interaction energy and elastic free energy.[46] The distance between the grafted points ($D = \sigma^{-1/2}$) was found to be smaller than the radius of gyration (R_g) of the PS chains in good solvent,[47] confirming the brush regime for PS (**ESI, S2**).

3.2 Bilayer formation

Once the monolayer is formed and provided that the excess of non-adsorbed copolymer remains in solution, the controlled addition of water will increase gradually the polarity of the solvent turning on the hydrophobic effect and triggering the interaction between free and grafted PS blocks (**Figure 1**). From a thermodynamic point of view, the addition of water translates into an increase in the Flory-Huggins PS-solvent interaction parameter (χ), namely a loss of solubility of the PS blocks. It is notorious that amphiphilic BCs form non-equilibrium structures when the solvent polarity of the medium changes.[48] It follows that BC self-assembly in bulk solution and by extension at solid-liquid interfaces is overly sensitive and dependent on processing parameters. Among them, the water content is most critical: it must be sufficient to confer amphiphilic properties to the BCs while avoiding their aggregation at surface, in particular with copolymers containing long PS blocks.

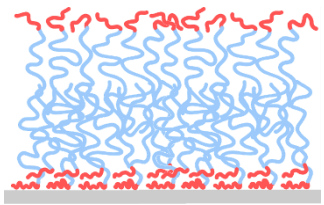

Figure 3. Illustration of the symmetric bilayers of PS-b-PAA bilayers.

The minimum water content to induce BC self-assembly, also called critical water content (cwc), was determined by light scattering in solution for each BC system. Low values of cwc were obtained, between 4 and 6%, highlighting the very hydrophobic nature of the PS blocks (**ESI, S3**).[49] In this range of water contents, the system is expected to be equilibrated, that is, a dynamic equilibrium between copolymer unimers and self-assembled structures exists. At higher water contents (> 10%), the chain mobility is drastically reduced due to lower concentration of DMF:THF in hydrophobic domains.[49] Then, the system becomes frozen and the subsequent addition of water should not alter its structural integrity. In solution, the different BCs investigated here self-assembled into crew-cut micelles when water was added in similar conditions to those used for bilayer formation (see below) (**ESI, S3**). Therefore, this disqualifies the BC compositions used here to form the bilayer through the vesicle spreading approach. The two-step self-assembly process was performed in a teflon trough of 17 cm x 1 cm x 2 cm using two syringe pumps for the injection and withdrawal of solutions, as shown in **Figure 3**.

First, the formation of the monolayer previously described was proceeded similarly by the immersion of APTES (or PAH)-modified substrates to the trough containing the BC solution in DMF:THF for 2 h. The second step was then performed by adding water from the left-side of the trough until the targeted cwc value was obtained. A small flow rate (50µL/min) was applied to ensure the self-assembly as close as possible to equilibrium conditions. Then, the system was equilibrated for 1h and extensively rinsed by continuous injection and withdrawing of water to remove bulk aggregates that were concomitantly formed during the bilayer assembly. The supported bilayers exposed to air or water present a rather continuous and smooth surface as observed by AFM (roughness < 1 nm), with an average thickness between 14 and 18 nm, more than twice thicker than the monolayers at the same condition. The difference is explained by the collapsed structure present in the monolayer, that does not occur in the case of the bilayer due to chain stretching.

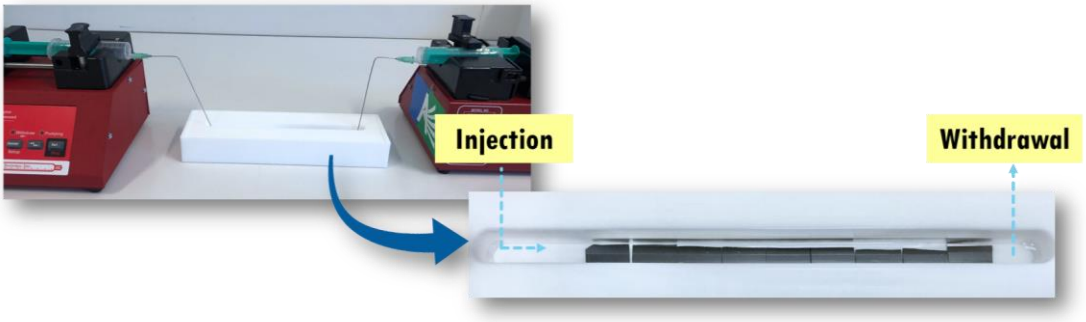

Figure 4. Illustration of the experimental set-up for the preparation of the solid-supported bilayers. Injection and withdraw pumps placed on the left and right sides of the Teflon trough, respectively.

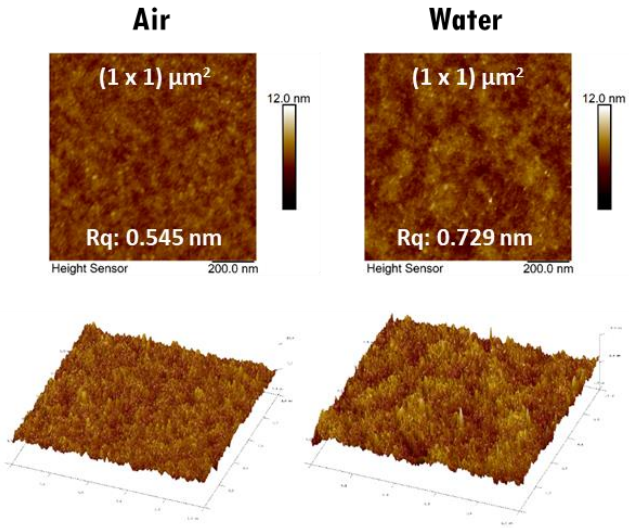

Figure 5. AFM images (PeakForce tapping mode) of the PS394-b-PAA58 bilayer in the dry and wet state.

No layer delineation phenomena at the liquid-air interface could be detected even when the molar mass of PS is below its critical mass (M_c = 31.2 10^3 g/mol) (**Figure 6**).[50] It suggests that hydrophobic interaction participate greatly to the molecular cohesion within the assembly. Also, we did not observe any significant difference in the morphology and thickness of the bilayer depending on the position of the substrate in the trough (**Figure 7**).

Similarly, the self-assembly process proved to be quite robust to some extent upon variation of initial conditions like the polymer concentration (0.3 g/L – 1 g/L), solvent (THF, DMF or a mixture), water content (5% - 10%) and incubation time before rinsing (1h -18h) (**ESI, S3**). It emphasizes that the bilayer formation must be quite fast once the composition of the medium meets the self-assembly criterion. Then, the bilayer remained stable against BC aggregation occurring in solution, especially during the rinsing step. This is an important aspect regarding the scale-up of the process. Only the pH of water showed some incidence on the bilayer characteristics. Namely the dried bilayer was found to be thicker for PS_{394}-*b*-PAA_{58} when the self-assembly was triggered at pH 11 (δ = 18 nm) than pH 7 (δ = 14.7 nm) (**ESI, S4**). This can be primarily attributed to the stretching of the PAA blocks on the bilayer surface forming a charged brush at pH 11 due to the high osmotic pressure of counterions.[51,52] Then, the drying step froze the system in such a conformation.

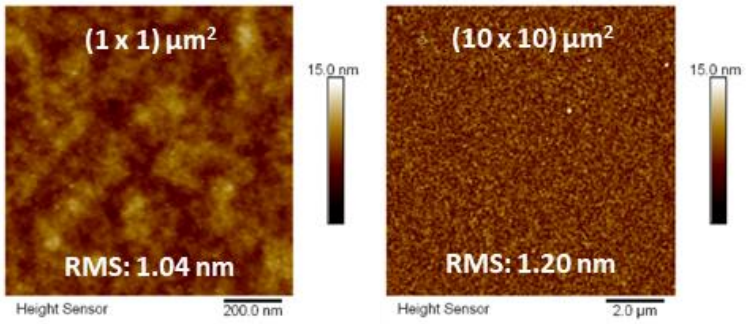

Figure 6. Height AFM images of PS_{182}-b-PAA_{58} bilayers.

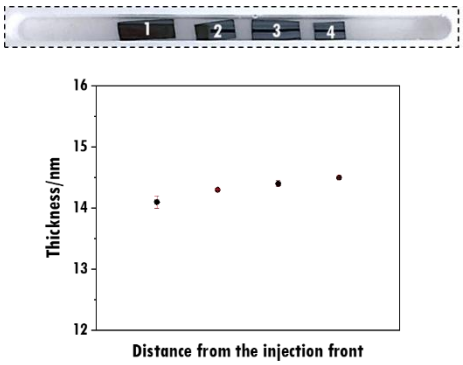

Figure 7. Illustration of the disposition of the samples in the trough (up) and respective thickness of the BC bilayers determined by ellipsometry (down).

3.3. Spectroscopic characterization of mono- and bilayers

A comparison between PS_{394}-*b*-PAA_{58} mono- and bilayers was done by PM-IRRAS (

Figure 8). One can observe, considering the peak areas, that the bilayer is more than 5 times the monolayer. As it is known, the orientation of the groups at the substrate highly influences the intensity of the absorption bands in PM-IRRAS measurements: the maximum absorption happens when the groups are oriented perpendicularly to the substrate, whereas a negligible absorption is measured when the groups are oriented parallel to the surface. The large increase of intensity observed for the bilayer could be then related to either a higher amount of PS groups and/or to a change of orientation of the PS chains. Indeed, as observed by AFM, a much higher grafting density is observed for the bilayers, as no dewetting takes place. One can imagine that the PS chains from the hydrophobic reservoir are much more stretched, and, thus, an increase in the intensity due to a change in orientation is reasonable. Additionally, the bilayer obviously presents another layer of BC, which will account for an increase on the intensity of the bands.

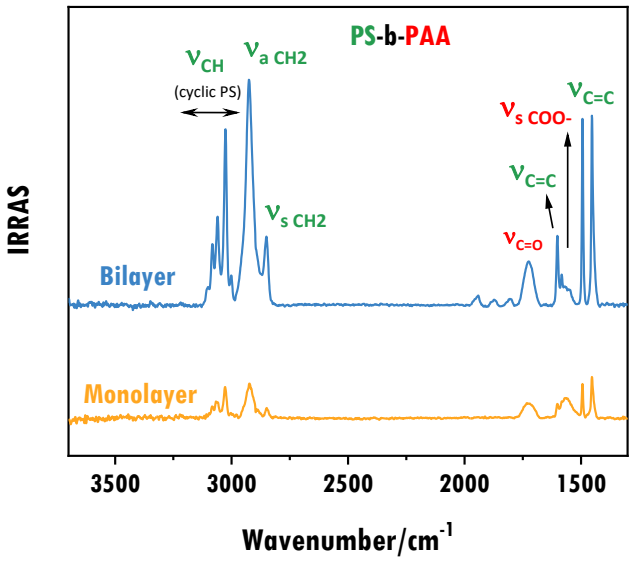

Figure 8. PM-IRRAS spectra of a PS_{394}-b-PAA_{58} mono- and bilayer.

3.4. Accessing the hydrophobic core of the bilayers with NR

Taking advantage of the isotopic contrast experiments available on neutron-based techniques, neutron reflectivity (NR) was performed with *a* PS_{394}-*b*-PAA_{58} bilayers prepared with BC containing a hydrogenated and/or deuterated PS block. Because the variation of the scattering length density (SLD) can be monitored trough the bilayer (in the z-direction), 2 different configurations were studied, in whose alternatively a deuterated (or hydrogenated) BC was used in the first step (monolayer formation) and a hydrogenated (or deuterated) BC was used at the second step (bilayer formation), allowing the generation of mixed hydrogenated/deuterated bilayers. NR curves of symmetric (PS_d-*b*-PAA and PS_h-*b*-PAA) or asymmetric

(PS_d-*b*-PAA/PS_h-*b*-PAA and PS_h-*b*-PAA/PS_d-*b*-PAA) bilayers are shown in

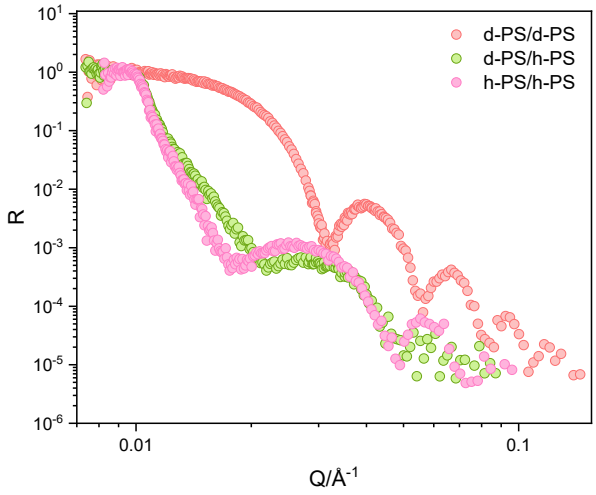

Figure 9.

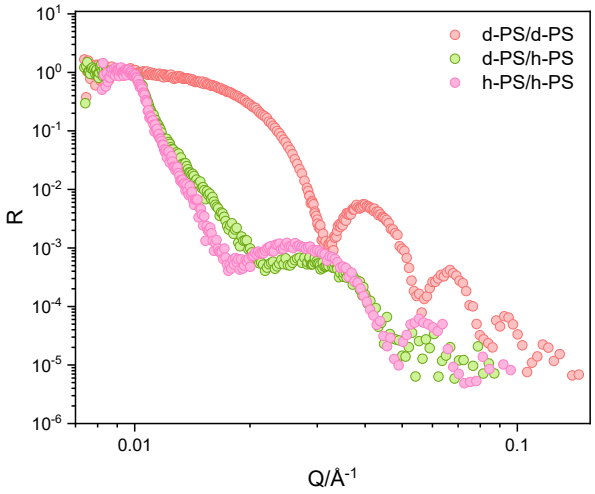

Figure 9. NR curves of PS_{394}-b-PAA_{58} bilayers of different fully hydrogenated and fully hydrogenated BC bilayers, and mixed hydrogenated/deuterated BC bilayers.

From the NR curves, the variation of the scattering length density (SLD) through the bilayer can be monitored. Since the SLD of the hole layer (measured by NR) is a sum of the partial contributions of each of the deuterated and hydrogenated layers:

$$\mathrm{SLD}_{total} = \mathrm{SLD}_{d-S}\,\phi(z)_{d-S} + \mathrm{SLD}_{h-S}\,\phi(z)_{h-S} \qquad \text{Eq. 2}$$

where $\phi(z)$ is the volume fraction at the z direction of deuterated and hydrogenated styrene monomers ($\phi(z)_{d\text{-}S} + \phi(z)_{h\text{-}S} = 1$), one can obtain the variation of the volume fraction of both hydrogenated and deuterated monomers as shown in

Figure 10.

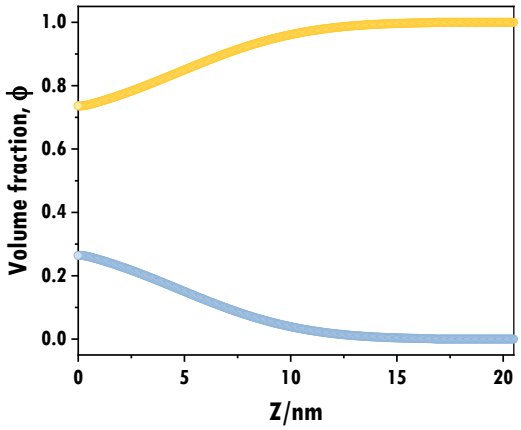

Figure 10. Variation of the volume fraction $\phi(z)$ of the asymmetric h/d bilayer.

At values very close to the substrate ($z \approx 0$), the volume fraction of the monomers coming from the top layer is far from being equal to zero. The absence of a pure contribution of the d-PS BC or h-PS BC could suggest a very pronounced interdigitation of the BC chains, reasonable with the fact that the monolayers present a rather low grafting density. Additionally, one can observe that the contributions are not even: when the monolayer was prepared with d-PS and the second layer with h-PS, the volume fraction of d-PS was around 0.25 close to the substrate, whereas a volume fraction of h-PS around 0.4 was found when the hydrogenated BC was used for the monolayer formation. We discovered, however, that instead of a very pronounced interdigitation of the lower and upper layers of block copolymers, the reason for the existence of a mixed monolayer of h-BC and d-BC is due to a densification of this lower monolayer with unimers that inserts into it just before BC self-assembly, i.e. in the early stages of water addition (below cwc). These results are described in a forthcoming publication.

3.5. Versatility of the self-assembly approach (SISAL)

3.5.1. Formation of asymmetric bilayers

This method of preparing block copolymer bilayers on a solid support also enables the fabrication of asymmetrical BC bilayers, where BCs containing the same glassy PS hydrophobic block but different hydrophilic blocks (PAA or poly-2-vinylpyridine, P2VP) are used to generate a bilayer with a different top surface, broadening the applications of this new approach. For example, smooth PS-b-PAA/PS-b-P2VP were successfully prepared (Figure 11**.A**) and were able to anchor citrate-coated gold nanoparticles (AuNPs) thanks to specific interactions between the hydrophilic block and the AuNPs coating.

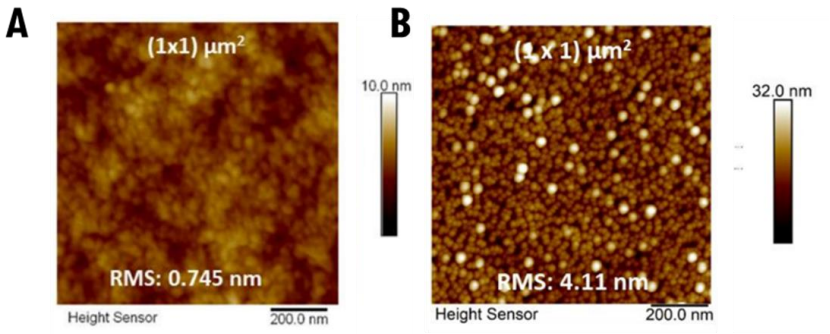

Figure 11. PS-b-PAA/PS-b-P2VP bilayers before a. and after b. incubation with (9 ± 5) citrate-modified AuNPs.

3.5.2. Encapsulation of actives: Gold nanoparticles

A major interest in the preparation of solid-supported bilayers lies in the encapsulation of actives on the hydrophobic reservoir. To illustrate the feasibility of asset encapsulation with our approach, we dispersed 5 nm of AuNPs in a PS-b-PAA solution and performed the same procedure for solid-supported BC bilayers as described above. BC bilayers prepared in the presence of AuNPs were thicker (~23 nm) but still presented a dense, smooth surface. The presence of AuNPs was confirmed by UV-VIS spectroscopy with the presence of SPR on samples of solid-supported BC bilayers with encapsulated AuNPs, in contrast to the negligible absorption associated with bare BC bilayers (

Figure 12).

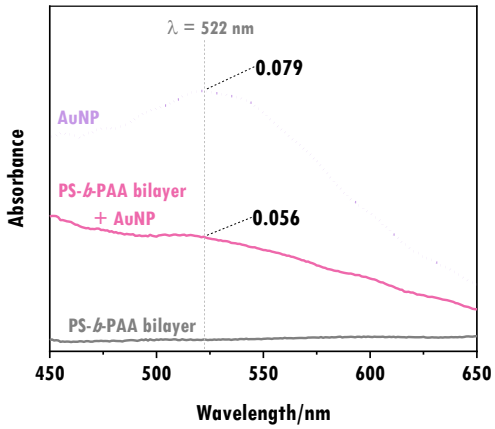

Figure 12. UV-Vis spectra of the AuNPs alone and PS394-b-PAA58 bilayers in the presence and absence of AuNPs.

After treatment with oxygen plasma, which removes organic matter from the bilayer, a distribution of isolated gold NPs was observed by AFM, confirming that these particles were not only present in the hydrophobic reservoir of the bilayer, but in a fairly organized manner.

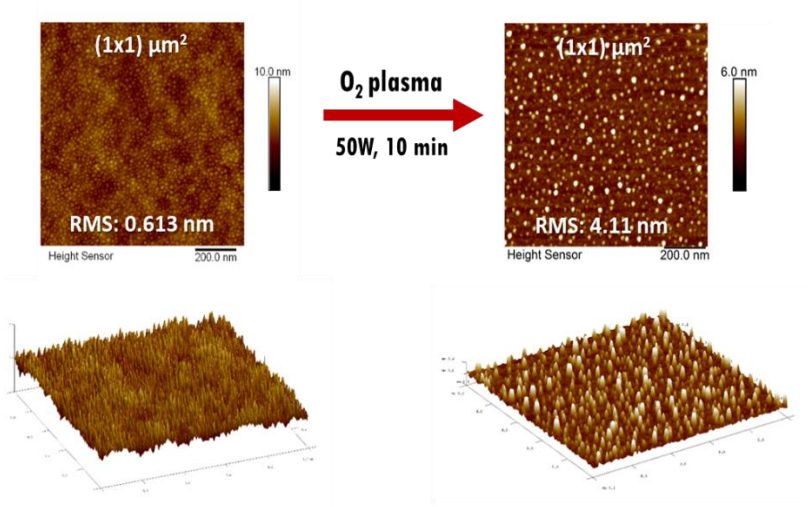

Figure 13. AFM images showing the surface organization of AuNP-loaded bilayer before (left) and after (right) oxygen plasma treatment.

As well as being excellent probes for the proof-of-concept of encapsulating actives in solid-supported BC bilayers, AuNPs could also be used to trigger temperature-induced opening of the BC bilayer and thus release the molecules of interest coencapsulated with them.

3.5.3. Formation of BC bilayers onto colloids

The formation of amphiphilic BC bilayers has also been extended to non-planar surfaces, in particular to the surface of colloidal substrates. Instead of amino-modified silicon wafers, amino-modified silicon dioxide nanoparticles (average diameter of 100 nm) were used (see SI for full characterization). As with planar surfaces, the assembly process was carried out in two stages involving, firstly, the formation of a PS394-b-PAA58 monolayer under non-selective solvent conditions using the same DMF:THF mixture as previously. Size distributions were determined by DLS for different weight ratios of SiO_2-

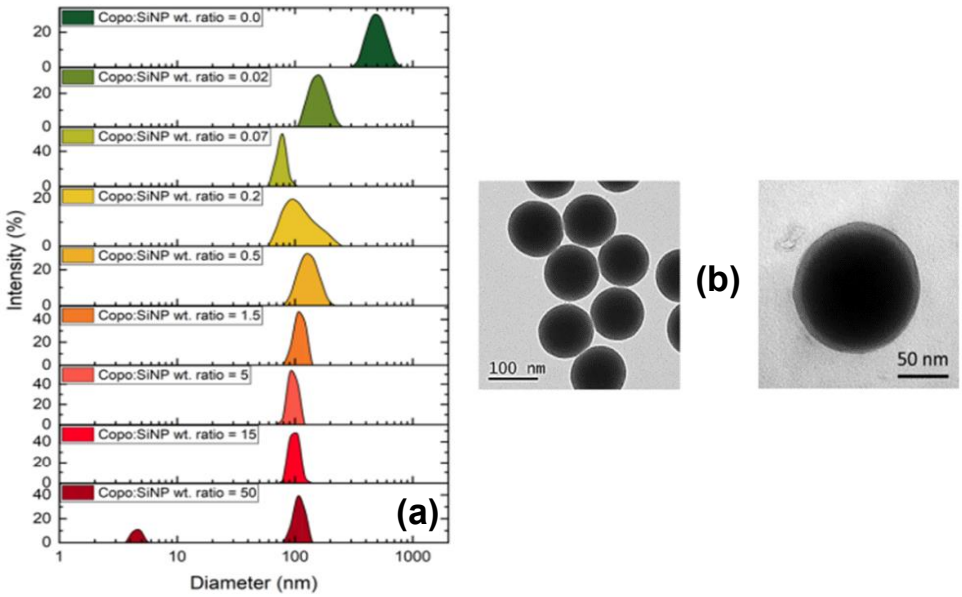

NPs to BCs (**a)**.

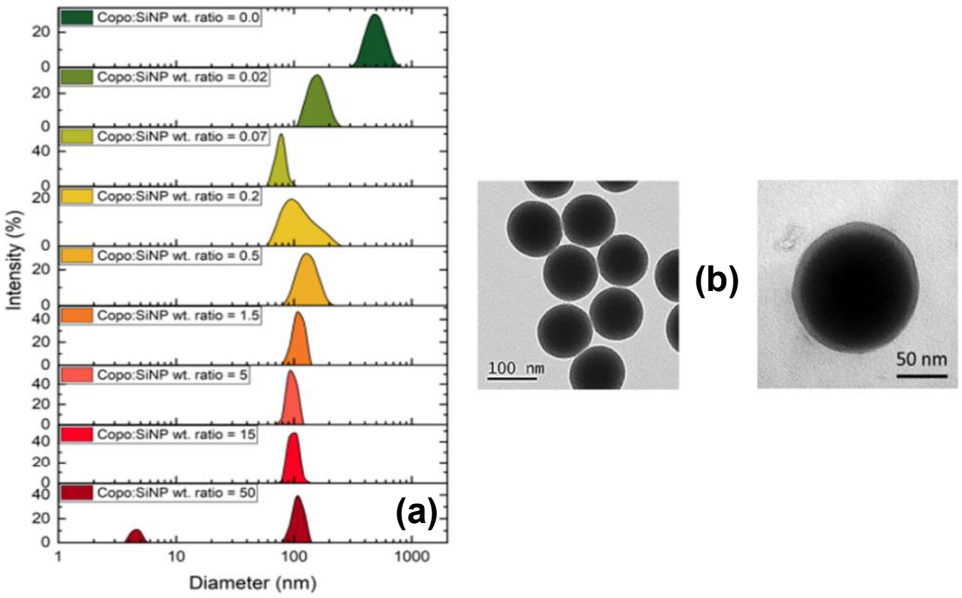

shows that the presence of copolymer in solution breaks up the nanoparticle aggregates. This is indirect evidence of the interaction of the surface amine groups with the acid groups of the copolymer. When the BC monolayer is formed, the improved stabilization due to BC at the surface allows better particle dispersion, with fewer aggregates, resulting in an apparently smaller particle size. In addition, it was possible to detect free polymer chains in solution at the highest mixing ratio (BC:NP SiO_2 = 50), demonstrating nanoparticle surface saturation. The formation of a BC monolayer on the particle surface was also observed by

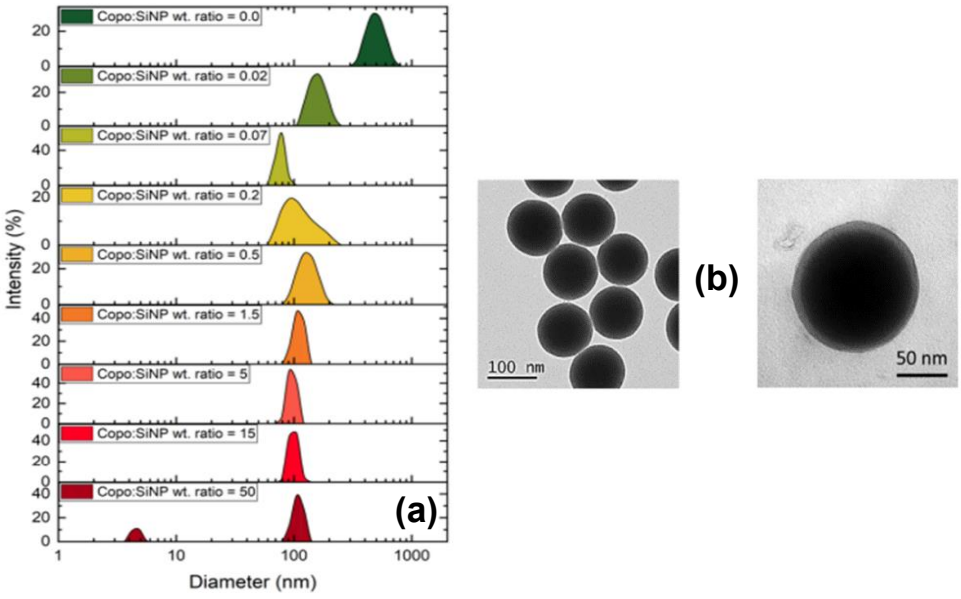

TEM, as shown in (**b)**. However, DLS cannot be used to accurately determine particle surface saturation, as the scattering intensity of silica nanoparticles is much greater than that of excess free copolymer.

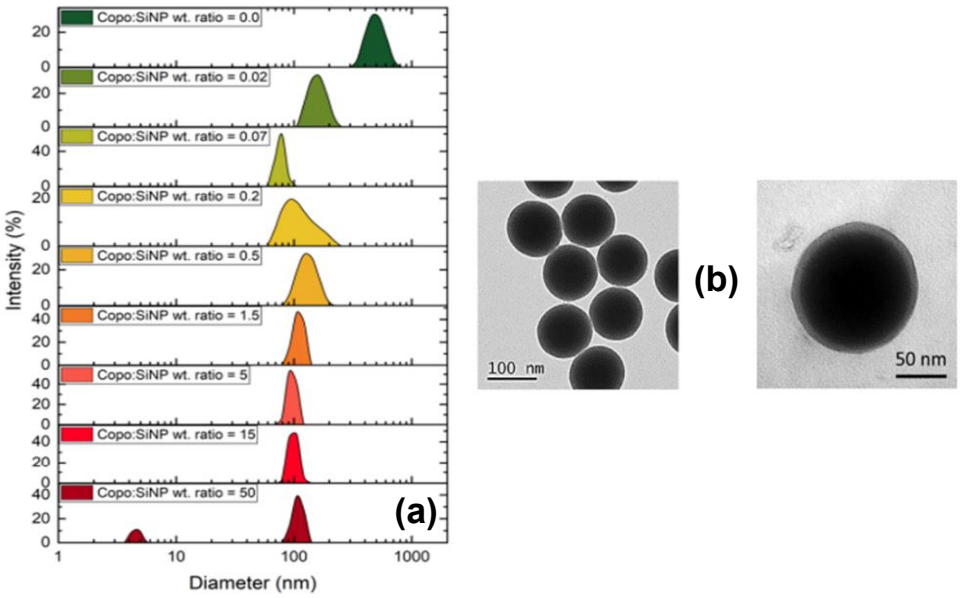

Figure 14. (a) Intensity-weighted size distribution of mixtures of amino-functionalized silicon dioxide nanoparticles and PS394-b-PAA58 BC prepared at different weight ratios (BC:SiO_2-NPs) in DMF:THF (80:20) without purification. **(b)** TEM images of the amine-modified SiO_2-NPs before (left) and after (right) coating with a monolayer of PS394-b-PAA58.

After the BC monolayer formation, water was added to switch the solvent polarity and, thus, trigger the formation of the second BC layer. The particles were then washed and rinsed by successive centrifugations in order to disperse them in water or in a neutral pH buffer. The nanoparticles were characterized at the end of each assembly step, which allowed to determine the optimal experimental conditions leading to the formation of the layer. As observed in **Figure 15 a**, size distributions determined by DLS seemed to remain practically constant for different BC:SiO_2-NP mixing ratios. However, a slight increase in particle size at increasing mixing ratios is observed. This can be related to the increase of the hydrodynamic radius of particles in relation with the build-up of the BC bilayer at particle surface. This was also seen in TEM images (**Figure 15 b**) where a difference in surface coverage is clearly obtained depending on the mixing ratio. For a BC:SiO_2-NP ratio of 15, a very homogeneous BC bilayer was formed. Importantly, the BC bilayer coating stabilized the particles against aggregation, resulting in particles that were fully dispersed in the medium. ~~However, the present conditions need to be further optimized as the formation of some particle clusters resulting from bilayer fusion was observed in some cases (result not shown). This should be avoided by further studying the influence of the particle concentration on the overall BC self-assembly process. The rate of water addition, which also remains to be studied, could also play a role.~~

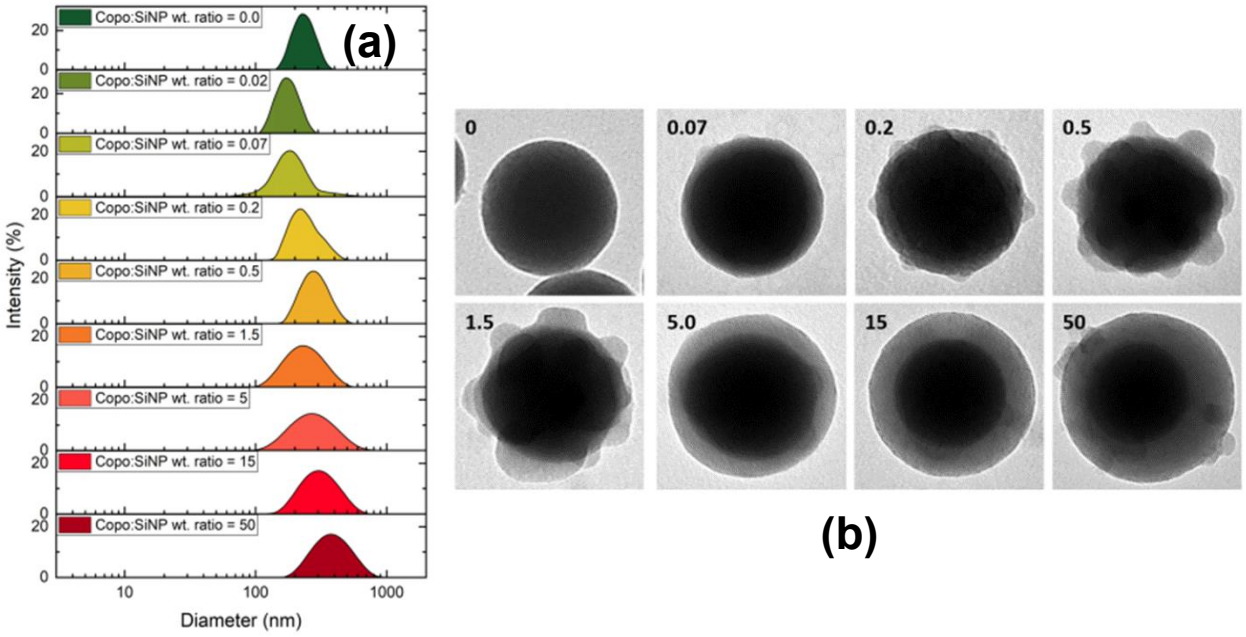

Figure 15. (a) Intensity-weighted size distribution of mixtures of silica nanoparticles and PS-b-PAA at different weight ratios after water addition to trigger the BC self-assembly. DLS analysis were performed after several centrifugation/dispersion cycles in water. **(b)**TEM pictures showing the formation of copolymer bilayer at the surface of silica nanoparticles for different BC:NP weight ratios, in water after purification of the excess copolymer by several centrifugation/resuspension cycles.

4. CONCLUSIONS

We have described a new method for fabricating bilayer-structured amphiphilic block copolymer films on solid substrates. The method is based on the general principle of self-assembly of amphiphilic molecules in aqueous media governed by the hydrophobic effect as described for surfactants. The novelty consists in reproducing the micellisation principle of amphiphilic block copolymers at a solid-liquid interface.

Unlike lipid bilayer self-assembly, which is generally achieved by fusing lipid vesicles (liposomes) to the surface of a solid substrate, our method involves BC self-assembly in two distinct steps: monolayer and bilayer formation. This is the strength and versatility of this new process, which can be used, in principle, on substrates of any shape and size (planar, colloidal, hollow), with a very wide variety of block copolymers well beyond those whose composition allows the formation of polymeric vesicles (polymersomes) in solution, and last but not least, allows the formation of asymmetric bilayers (**Figure 16**).

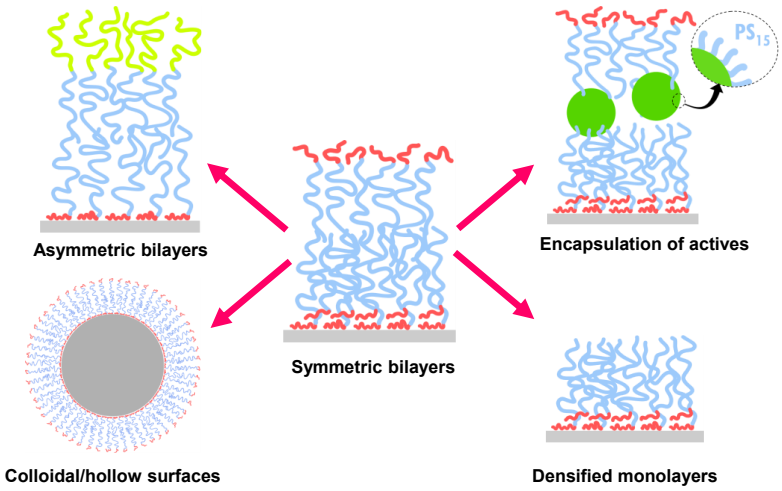

Figure 16. Potential and versatility of the SISAL surface-induced self-assembly approach proposed in this work.

Finally, the SISAL approach complements and enriches existing amphiphilic copolymer self-assembly methods already available in the literature (**Table 1**).

	LB	VF	SALB	**SISAL**
Easy protocol/instrumentation	✗	✓	✓	✓
Large macroscopic substrates	✗	✓	✓	✓
Colloidal or hollow substrates	✗	✓	✓	✓
Variety of BC composition	✓	✗	✗	✓
Symmetric and asymmetric bilayers	✓	✗	✗	✓
Suitable for scale up	✗	✓	✓	✓

Table 2. Advantages and disadvantages of amphiphilic block copolymer self-assembly methods available in the literature compared with the SISAL approach presented in this work. LB : Langmuir-Blodgett deposition, VF : Vesicle fusion, SALB : Solvent-assisted Lipid Bilayer.

5. REFERENCES

1 Forster, S. & Antonietti, M. Amphiphilic block copolymers in structure-controlled nanomaterial hybrids. *Advanced Materials* **10**, 195-+, doi:10.1002/(sici)1521-4095(199802)10:3<195::Aid-adma195>3.0.Co;2-v (1998).

2 Bates, F. S. & Fredrickson, G. H. Block copolymers - Designer soft materials. *Physics Today* **52**, 32-38, doi:10.1063/1.882522 (1999).

3 Lodge, T. P. Block copolymers: Past successes and future challenges. *Macromolecular Chemistry and Physics* **204**, 265-273, doi:10.1002/macp.200290073 (2003).

4 Hamley, I. W. Nanostructure fabrication using block copolymers. *Nanotechnology* **14**, R39-R54, doi:10.1088/0957-4484/14/10/201 (2003).

5 Riess, G. Micellization of block copolymers. *Progress in Polymer Science* **28**, 1107-1170, doi:10.1016/s0079-6700(03)00015-7 (2003).
6 Ruzette, A. V. & Leibler, L. Block copolymers in tomorrow's plastics. *Nature Materials* **4**, 19-31, doi:10.1038/nmat1295 (2005).
7 Segalman, R. A. Patterning with block copolymer thin films. *Materials Science & Engineering R-Reports* **48**, 191-226, doi:10.1016/j.mser.2004.12.003 (2005).
8 Darling, S. B. Directing the self-assembly of block copolymers. *Progress in Polymer Science* **32**, 1152-1204, doi:10.1016/j.progpolymsci.2007.05.004 (2007).
9 Bang, J., Jeong, U., Ryu, D. Y., Russell, T. P. & Hawker, C. J. Block Copolymer Nanolithography: Translation of Molecular Level Control to Nanoscale Patterns. *Advanced Materials* **21**, 4769-4792, doi:10.1002/adma.200803302 (2009).
10 Mai, Y. & Eisenberg, A. Self-assembly of block copolymers. *Chemical Society Reviews* **41**, 5969-5985, doi:10.1039/C2CS35115C (2012).
11 Luo, M. & Epps, T. H. Directed Block Copolymer Thin Film Self-Assembly: Emerging Trends in Nanopattern Fabrication. *Macromolecules* **46**, 7567-7579, doi:10.1021/ma401112y (2013).
12 Cummins, C. *et al.* Enabling future nanomanufacturing through block copolymer self-assembly: A review. *Nano Today* **35**, doi:10.1016/j.nantod.2020.100936 (2020).
13 Blanazs, A., Armes, S. P. & Ryan, A. J. Self-Assembled Block Copolymer Aggregates: From Micelles to Vesicles and their Biological Applications. *Macromolecular Rapid Communications* **30**, 267-277, doi:https://doi.org/10.1002/marc.200800713 (2009).
14 Discher, B. M. *et al.* Polymersomes: Tough vesicles made from diblock copolymers. *Science* **284**, 1143-1146, doi:10.1126/science.284.5417.1143 (1999).
15 Discher, D. E. & Ahmed, F. in *Annual Review of Biomedical Engineering* Vol. 8 *Annual Review of Biomedical Engineering* 323-341 (2006).
16 Goertz, M. P., Marks, L. E. & Montano, G. A. Biomimetic Mono layer and Bilayer Membranes Made From Amphiphilic Block Copolymer Micelles. *Acs Nano* **6**, 1532-1540, doi:10.1021/nn204491q (2012).
17 Kowal, J., Zhang, X., Dinu, I. A., Palivan, C. G. & Meier, W. Planar Biomimetic Membranes Based on Amphiphilic Block Copolymers. *Acs Macro Letters* **3**, 59-63, doi:10.1021/mz400590c (2014).
18 Chimisso, V., Maffeis, V., Hürlimann, D., Palivan, C. G. & Meier, W. Self-Assembled Polymeric Membranes and Nanoassemblies on Surfaces: Preparation, Characterization, and Current Applications. *Macromolecular Bioscience* **20**, 1900257, doi:https://doi.org/10.1002/mabi.201900257 (2020).
19 Bermudez, H., Brannan, A. K., Hammer, D. A., Bates, F. S. & Discher, D. E. Molecular weight dependence of polymersome membrane structure, elasticity, and stability. *Macromolecules* **35**, 8203-8208, doi:10.1021/ma020669l (2002).
20 Le Meins, J. F., Sandre, O. & Lecommandoux, S. Recent trends in the tuning of polymersomes' membrane properties. *Eur. Phys. J. E* **34**, 17, doi:10.1140/epje/i2011-11014-y (2011).
21 Belegrinou, S. *et al.* Biomimetic supported membranes from amphiphilic block copolymers. *Soft Matter* **6**, 179-186, doi:10.1039/B917318H (2010).
22 Zhang, X., Fu, W., Palivan, C. G. & Meier, W. Natural channel protein inserts and functions in a completely artificial, solid-supported bilayer membrane. *Scientific Reports* **3**, 2196, doi:10.1038/srep02196 (2013).
23 Rakhmatullina, E. & Meier, W. Solid-supported block copolymer membranes through interfacial adsorption of charged block copolymer vesicles. *Langmuir* **24**, 6254-6261, doi:10.1021/la8003068 (2008).
24 Dorn, J., Belegrinou, S., Kreiter, M., Sinner, E.-K. & Meier, W. Planar Block Copolymer Membranes by Vesicle Spreading. *Macromolecular Bioscience* **11**, 514-525, doi:https://doi.org/10.1002/mabi.201000396 (2011).
25 Yang, Y.-L., Tsao, H.-K. & Sheng, Y.-J. Solid-supported polymer bilayers formed by coil–coil block copolymers. *Soft Matter* **12**, 6442-6450, doi:10.1039/C6SM00741D (2016).
26 Hohner, A. O., David, M. P. C. & Rädler, J. O. Controlled solvent-exchange deposition of phospholipid membranes onto solid surfaces. *Biointerphases* **5**, 1-8, doi:10.1116/1.3319326 (2010).
27 Tabaei, S. R. *et al.* Biomembrane Fabrication by the Solvent-assisted Lipid Bilayer (SALB) Method. *J Vis Exp*, 53073, doi:10.3791/53073 (2015).

28 Ferhan, A. R. *et al.* Solvent-assisted preparation of supported lipid bilayers. *Nature Protocols* **14**, 2091-2118, doi:10.1038/s41596-019-0174-2 (2019).

29 Jackman, J. A. & Cho, N.-J. Supported Lipid Bilayer Formation: Beyond Vesicle Fusion. *Langmuir* **36**, 1387-1400, doi:10.1021/acs.langmuir.9b03706 (2020).

30 Khalil, R. A. & Zarari, A.-H. A. Theoretical estimation of the critical packing parameter of amphiphilic self-assembled aggregates. *Applied Surface Science* **318**, 85-89, doi:10.1016/j.apsusc.2014.01.046 (2014).

31 Decher, G. Fuzzy nanoassemblies: Toward layered polymeric multicomposites. *Science* **277**, 1232-1237, doi:10.1126/science.277.5330.1232 (1997).

32 Bui, L. *et al.* Encapsidation of RNA-Polyelectrolyte Complexes with Amphiphilic Block Copolymers: Toward a New Self-Assembly Route. *Journal of the American Chemical Society* **134**, 20189-20196, doi:10.1021/ja310397j (2012).

33 Schreiber, F. Structure and growth of self-assembling monolayers. *Progress in Surface Science* **65**, 151-256, doi:10.1016/s0079-6816(00)00024-1 (2000).

34 El'tekov, A. Y., El'tekova, N. A. & El'tekov, Y. A. Thin-layer chromatography in the investigation of polystyrene macromolecule interaction with nanoporous silica. *Protection of Metals and Physical Chemistry of Surfaces* **50**, 45-48, doi:10.1134/s2070205114010031 (2014).

35 Marques, C. M. & Joanny, J. F. Block copolymer adsorption in a nonselective solvent. *Macromolecules* **22**, 1454-1458, doi:10.1021/ma00193a075 (1989).

36 Fleer, G. J., Cohen Stuart, M. A., Scheutjens, J. M. H. M., Cosgrove, T. & Vincent, B. *Polymers at interfaces*. (Springer Science+Business Media, B.V., 1998).

37 Parsonage, E., Tirrell, M., Watanabe, H. & Nuzzo, R. G. Adsorption of poly(2-vinylpyridine)-poly (styrene) block copolymers from toluene solutions. *Macromolecules* **24**, 1987-1995, doi:10.1021/ma00008a041 (1991).

38 Li, Y., Pham, J. Q., Johnston, K. P. & Green, P. F. Contact Angle of Water on Polystyrene Thin Films: Effects of CO2 Environment and Film Thickness. *Langmuir* **23**, 9785-9793, doi:10.1021/la0636311 (2007).

39 Good, R. J. & Kotsidas, E. D. The contact angle of water on polystyrene: A study of the cause of hysteresis. *Journal of Colloid and Interface Science* **66**, 360-362, doi:https://doi.org/10.1016/0021-9797(78)90317-X (1978).

40 Spatz, J. P., Möller, M., Noeske, M., Behm, R. J. & Pietralla, M. Nanomosaic Surfaces by Lateral Phase Separation of a Diblock Copolymer. *Macromolecules* **30**, 3874-3880, doi:10.1021/ma9607372 (1997).

41 Maas, J. H., Cohen Stuart, M. A., Sieval, A. B., Zuilhof, H. & Sudhölter, E. J. R. Preparation of polystyrene brushes by reaction of terminal vinyl groups on silicon and silica surfaces. *Thin Solid Films* **426**, 135-139, doi:https://doi.org/10.1016/S0040-6090(03)00033-6 (2003).

42 Alexander, S. ADSORPTION OF CHAIN MOLECULES WITH A POLAR HEAD A-SCALING DESCRIPTION. *Journal De Physique* **38**, 983-987, doi:10.1051/jphys:01977003808098300 (1977).

43 de Gennes, P. G. Conformations of Polymers Attached to an Interface. *Macromolecules* **13**, 1069-1075, doi:10.1021/ma60077a009 (1980).

44 de Gennes, P. G. Polymers at an interface; a simplified view. *Advances in Colloid and Interface Science* **27**, 189-209, doi:https://doi.org/10.1016/0001-8686(87)85003-0 (1987).

45 Auroy, P., Auvray, L. & Léger, L. Characterization of the brush regime for grafted polymer layers at the solid-liquid interface. *Physical Review Letters* **66**, 719-722, doi:10.1103/PhysRevLett.66.719 (1991).

46 Milner, S. T. POLYMER BRUSHES. *Science* **251**, 905-914, doi:10.1126/science.251.4996.905 (1991).

47 Cotton, J. P. Polymer excluded volume exponent v : An experimental verification of the n vector model for n = 0. *J. Physique Lett.* **41**, 231-234 (1980).

48 Zhang, L. & Eisenberg, A. Thermodynamic vs kinetic aspects in the formation and morphological transitions of crew-cut aggregates produced by self-assembly of polystyrene-b-poly(acrylic acid) block copolymers in dilute solution. *Macromolecules* **32**, 2239-2249, doi:10.1021/ma981039f (1999).

49 Zhang, L., Shen, H. & Eisenberg, A. Phase Separation Behavior and Crew-Cut Micelle Formation of Polystyrene-b-poly(acrylic acid) Copolymers in Solutions. *Macromolecules* **30**, 1001-1011, doi:10.1021/ma961413g (1997).

50 Fetters, L. J., Lohse, D. J. & Colby, R. H. in *Physical Properties of Polymers Handbook* (ed James E. Mark) 447-454 (Springer New York, 2007).

51 Pincus, P. Colloid stabilization with grafted polyelectrolytes. *Macromolecules* **24**, 2912-2919, doi:10.1021/ma00010a043 (1991).

52 Zhulina, E. B. & Borisov, O. V. Polyelectrolytes Grafted to Curved Surfaces. *Macromolecules* **29**, 2618-2626, doi:10.1021/ma9515801 (1996).